Supplementary Material

Quantitative *in situ* synchrotron x-ray analysis of the ALD/MLD growth of transition metal dichalcogenide TiS_2 ultrathin films

Ashok-Kumar Yadav[1,], Weiliang Ma[2], Petros Abi Younes[3,4], Gianluca Ciatto[1,*], Nicolas Gauthier[4], Evgeniy Skopin[3], Elsje Alessandra Quadrelli[5], Nathanaelle Schneider[2], Hubert Renevier[3]*

[1]Synchrotron SOLEIL, Beamline SIRIUS, Saint-Aubin, F-91192, Gif sur Yvette, France.

[2]IPVF (UMR 9006), Institut Photovoltaïque d'Ile-de-France, F-91120 Palaiseau, France.

[3]Univ. Grenoble Alpes, CNRS, Grenoble-INP, LMGP, F-38000 Grenoble, France

[4]Univ. Grenoble Alpes, CEA, LETI, F-38000 Grenoble, France.

[5]Université de Lyon, IRCELYON, CNRS, F-69100 Villeurbanne, France.

1. XAFS analysis:

X-ray Absorption Spectroscopy (XAS) measurements were conducted at the Ti and S K-edges. The absorption coefficient is obtained using the relation $\mu = c * I_f / I_0$, where I_f is the fluorescence intensity obtained from the four channel Si-drift detector and I_0 *is* incident flux, c is a constant. Since we are dealing with ultrathin films, the fluorescence yield is proportional to the absorption coefficient. The local structure surrounding the absorbing atom is determined through quantitative analysis of EXAFS spectra. To address the oscillations in the absorption spectra, it has been necessary to extract the atomic background as follows: [1]:

$$\chi(E) = \frac{\mu(E) - \mu_0(E)}{\Delta\mu_0(E_0)} \tag{1}$$

where, E_0 is absorption edge energy, $\mu_0(E_0)$ is the bare atom background and $\Delta\mu_0(E_0)$ is the step in $\mu(E)$ value at the absorption edge. To obtain the wave number dependent background-extracted $\chi(k)$ function, the energy-dependent absorption coefficient $\chi(E)$ was converted using the following relation:

$$K = \sqrt{\frac{2m(E - E_0)}{\hbar^2}} \tag{2}$$

where, m is the electron mass. $\chi(k)$ is weighted by k^2 to amplify the oscillation at high k and the $\chi(k)k^2$ functions are Fourier transformed to generate the $\chi(R)$ versus R plots in terms of the real distances from the center of the absorbing atom. The bond length, coordination number, and disorder factors for each scattering path obtained from the potential crystal structures are utilized as fitting parameters. The total number of fitting variables is monitored in accordance with Nyquist criteria [2]. The quality of the fitting is assessed using statistical parameters and reasonable fitting results [3].

2. Linear combination fitting

The linear combination fittings have been carried out using Athena. The fittings have been carried in the range of -20 to +30 eV with respect to E_0. The LCF also has been carried out on $\chi(k)$ spectra at Ti K-edge in the range of 2-10 $Å^{-1}$ to validate the contribution of included components. The obtained variation (maximum 10% for some initial spectra) found between EXAFS and XANES LCF is due to the relatively high noise in $\chi(k)$ for initial growth cycles at higher wave number due to low concentration of the sample. Three components, which were sufficient to fit the spectra measured during the growth and annealing followed by cooling have been used for LCF. The initial cycle (half ALD/MLD cycle (cy0.5) at Ti K-edge and first ALD/MLD cycle (cy1) for S K-edge), an intermediate phase Ti-thiolate (cy40) and the final target structure TiS_2 are used as three LCF components as their selection justified in discussion section of main text.

3. Amorphous TiS_2 XANES simulations

The Amorphous TiS_2 structures have been optimized using Molecular dynamics. To generate the amorphous phase, the melting-quenching approach has been performed within *ab initio* molecular dynamics (AIMD). A 4×4×3 supercell of TiS_2 with 144 atoms was generated from a fully relaxed TiS_2 crystal. First, the supercell was kept at ambient temperature (300K) for 50 fs. Then the temperature increased to target temperature within a short time (50 fs). The supercell was held in the target temperate for 2000 fs before quenching to ambient temperature within 50 fs. To give a detailed evolution of amorphous level, the target temperature was set from 1000K to 5000K with a step of 200K, where the melting point of TiS_2 is higher than 1273K [4]. The amorphous

phase generated with different melting temperature is illustrated in figure S1. The level of amorphous states increases with the increasing of AIMD temperature. The XANES simulations have been performed using FDMNES for TiS_2 amorphous structures. The aim of the different simulated structures was to look for a better agreement with the experimental XAFS spectra of the annealed samples at the Ti K-edge, in particular to understand if the reduction of the peak around 10 eV compared to crystalline TiS_2 could be due to the formation of amorphous TiS_2 instead of nano-crystalline one. It can be observed from the spectra given in figure S2 that the pre-edge intensities are diminished with temperature, however the peak around 10 eV never transforms into a shoulder. It can be seen from figure S2 that even for the amorphous structure obtained using the highest melting temperature (3400 K) and maximum frequency (2000fs), this peak around 10 eV is always present. The permanence of this peak even in amorphous TiS_2 structures suggests that the formation of amorphous TiS_2 is not a good explication for the residual dissimilarity between the spectra of our annealed samples at the Ti K-edge and crystalline TiS_2. On the contrary, the spectra of annealed samples can be well simulated by assuming a mixture between crystalline TiS_2 and a “S-free” Ti compound, as shown in the main manuscript.

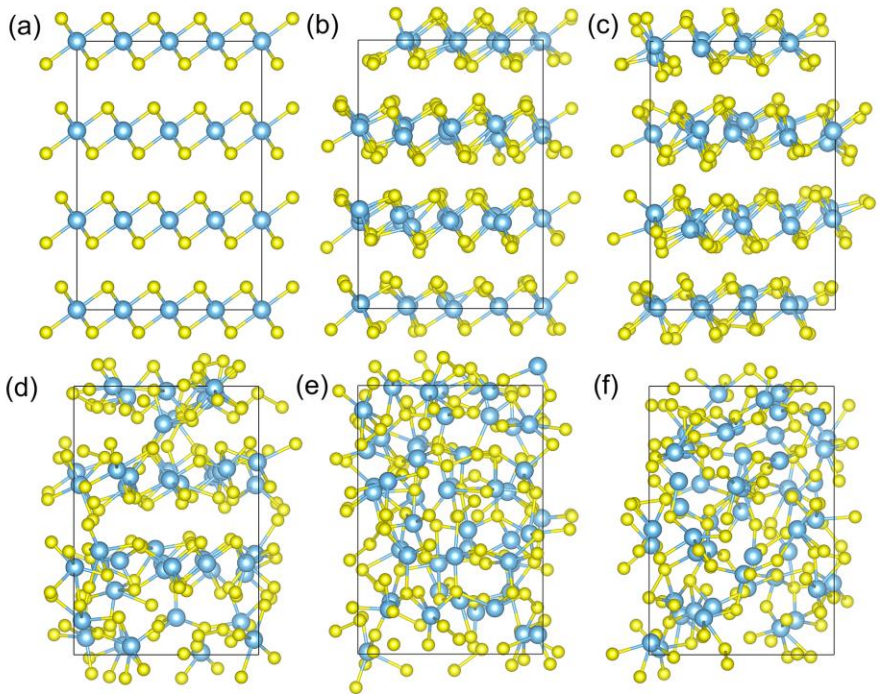

Figure S 1: Simulated amorphous states of TiS_2 with a 4×4×3 supercell under different temperature of 0K (a), 2200K (b), 2600K (c), 3000K (d), 3400K (e) and 3800K (f).

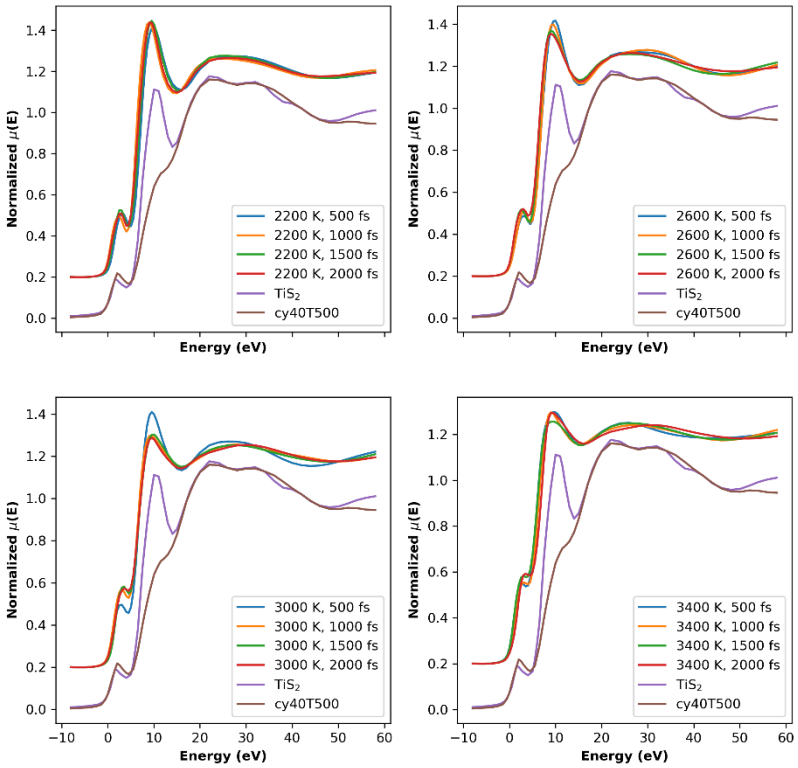

Figure S 2: Simulated XANES spectra using FDMNES of amorphous TiS_2 structures. The spectra of crystalline TiS_2 and cy40T500 (annealed after 40 ALD/MLD cycle growth) are vertically shifted for better illustration.

4. S/Ti XRF ratio and S losses

During the growth process, element-specific *in situ* analysis was performed by monitoring Ti and S X-ray fluorescence (XRF) at each successive ALD and MLD step. This allowed quantification of the amount of Ti and S deposited on the sample surface. The S/Ti XRF ratio, up to the completion of 40 ALD/MLD cycles and calibrated with XPS results, is shown in Figure S3. Overall, the S/Ti ratio initially exhibits a brief transient regime of growth where the ratio is

relatively low. This is also reflected in the absence of a coordination peak for the initial few cycles in the Fourier transform EXAFS spectra, as shown in the manuscript.

The recorded absorption spectra at the S K-edge during the growth of 40 ALD/MLD cycles, as well as their annealing and cooling steps, are shown in Figure S4. The normalized spectra are presented in Figure S5. The loss of sulfur during the annealing and cooling of the sample can be observed in Figure S4, where the intensity of the absorption spectrum of cy40T500 significantly reduces compared to the cy40 sample. Further reduction in absorption can be seen for the cy40Tcool spectrum. Evidence of sulfur loss during the annealing and cooling process is also apparent in Figure S6, where a significant reduction in the S/Ti ratio can be observed.

5. Quantitively determination of bond lengths and interatomic distances via XAS

The Ti-O/N and Ti-S bond lengths obtained from the EXAFS analysis carried out at Ti K-edge for the spectra measured during the growth, annealing and cooling are plotted in figure S7. The best fittings obtained at the Ti K-edge are represented in figure S8. The scattering amplitude for the Ti-O/N and Ti-S coordination have been calculated using the DFT optimized structure and TiS_2 crystal structures [5]. In the optimized mono-podal configuration, where the surface is completely covered with OH groups, two irreducible adsorption positions exist for TDMAT. The TDMAT molecule is bonded to the outermost O atom, forming the first Ti-O bond, and subsequently generates a second Ti-O bond with the nearest O atom connected to a different Si atom. The first coordination peak at 1.5 Å corresponding to the Ti-O/N coordination and the gradually growing second coordination peak around 2.1 Å represents Ti-S coordination. The fitting results are given in table S2.

The presence of Ti-N bond lengths supports the interpretation that there are two separate local environments around the Ti atom, after annealing. The analysis of the S edge revealed both S-Ti and S-S coordinations for the annealed sample (Table S3). Figure S7 shows the variation of Ti-O/N and Ti-S bond lengths during ALD/MLD growth, annealing, and cooling, with a decreasing trend being observed for Ti-S bond lengths. The Ti-S bond lengths obtained for cy1 have been found to be relatively longer than Ti-S bond lengths in TiS_2 (2.45 Å) [6]. The EXAFS analysis has provided an average bond length for all possible sulfur coordination surrounding the Ti atoms. Initially, the longer bond lengths could be related to either unreacted S or the average distance between both S atoms connected to the Ti via EDT. The Ti-S bond lengths for cy40 also corroborate with the thiolate structures [7]. It is also interesting to note the low amplitude of all the peaks after 2.5 Å in the Fourier transform spectra (figure S8), which indicates the absence of long-range order during the growth of the sample.

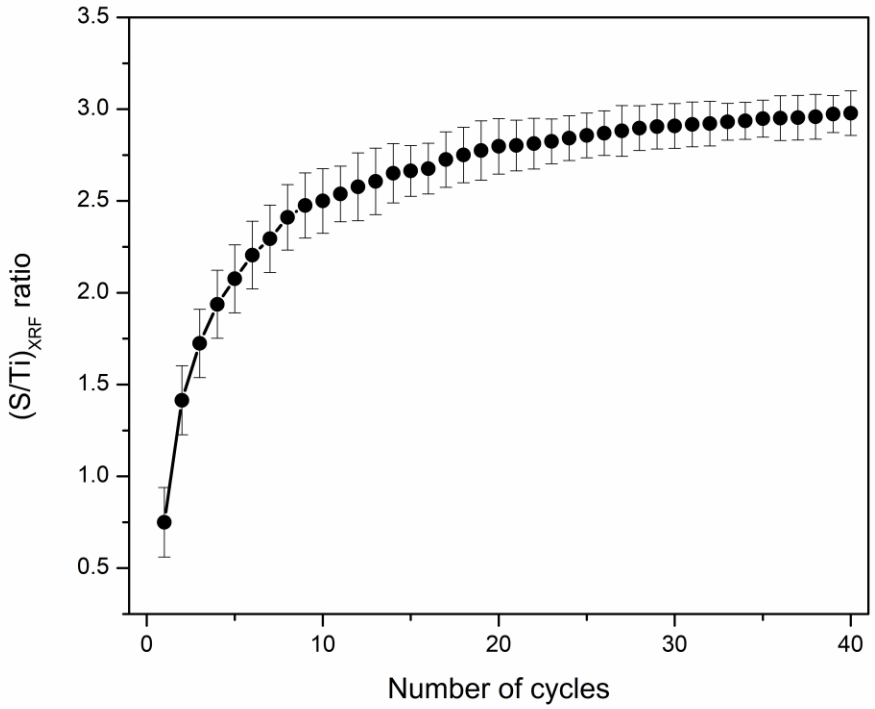

Figure S3: S/Ti XRF ratio during the growth of 40 ALD/MLD cycles of Ti-thiolate calibrated with XPS.

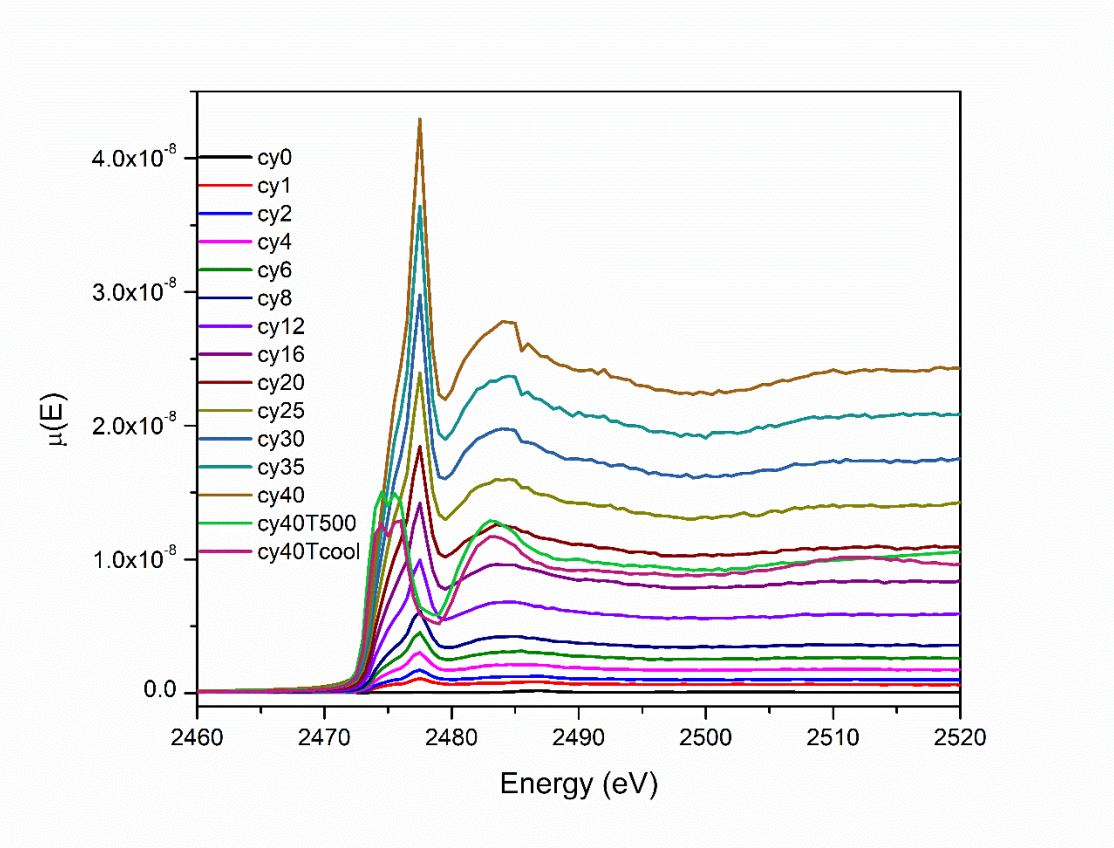

Figure S 4: Absorption spectra for different ALD/MLD growth cycles. The intensity of the absorption is clearly depending on the concentration of sulfur in the sample. The contamination (cy0) signal is negligible compared to the actual signal from the ALD/MLD cycles.

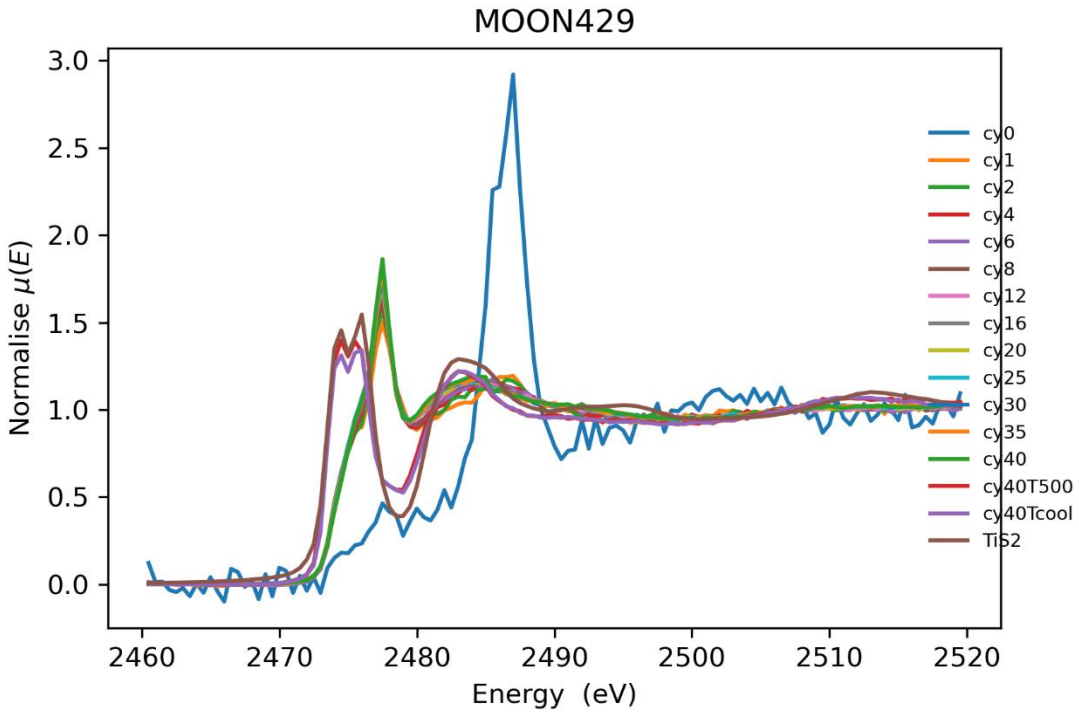

Figure S 5: Normalized absorption spectra for different ALD/MLD growth cycles. The intensity of the absorption is clearly depending on the concentration of sulfur in the sample. The contamination (cy0) signal is negligible compared to the actual signal from the ALD/MLD cycles.

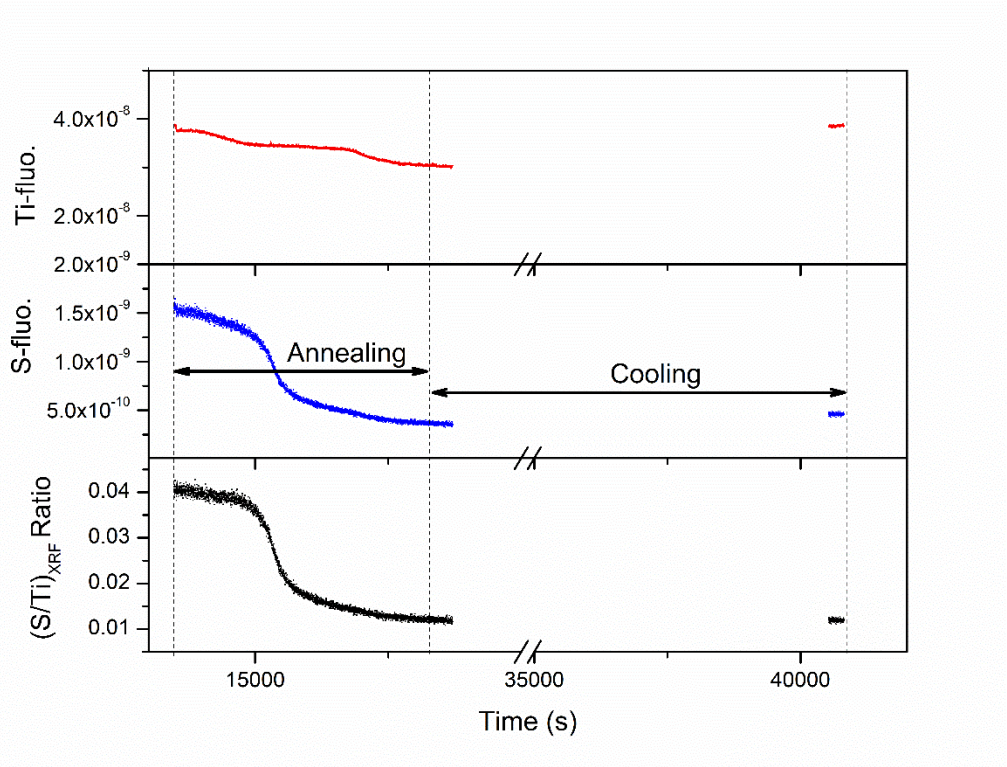

Figure S 6: (top) Ti-(Kα) fluorescence, (middle) S-(Kα) fluorescence and (bottom) S/Ti ratio obtained during the ALD/MLD growth, annealing and cooling of the sample.

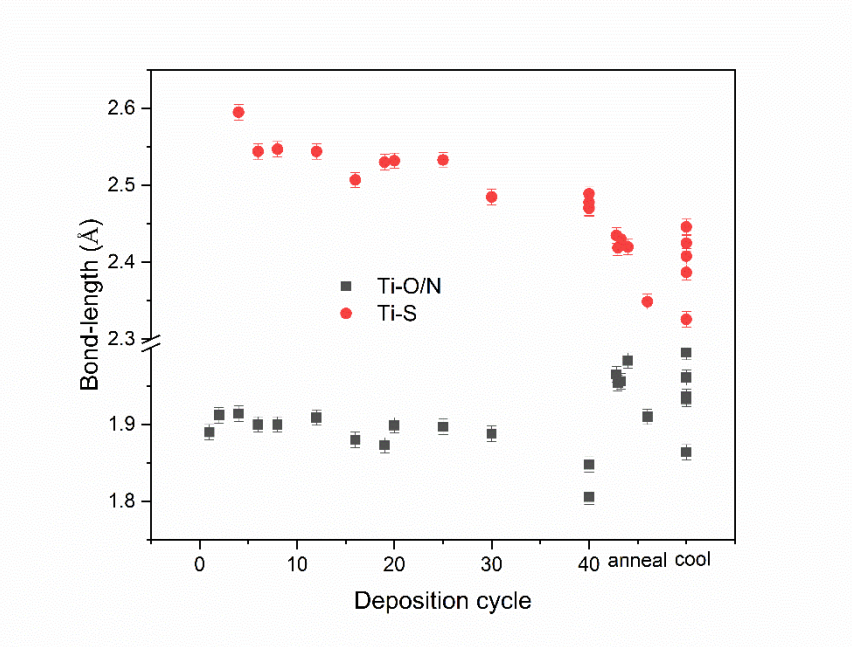

Figure S 7: Variation of Ti-O/N and Ti-S bond lengths with ALD/MLD growth cycles, annealing and cooling. The annealing and cooling on horizontal axis represent measurements carried out at different temperatures for different growths.

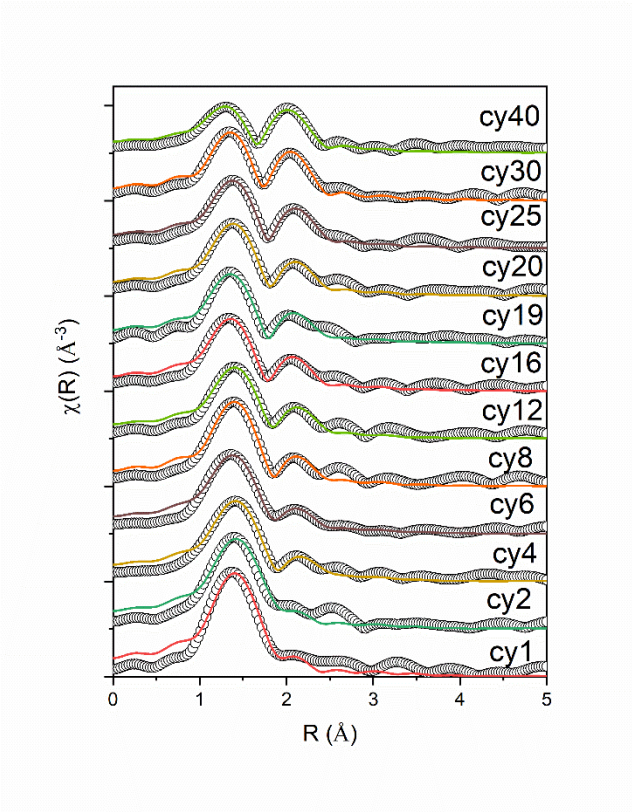

Figure S 8: The Fourier transform EXAFS spectra (scatter points) and its corresponding fits (solid line) for different ALD/MLD deposition cycles.

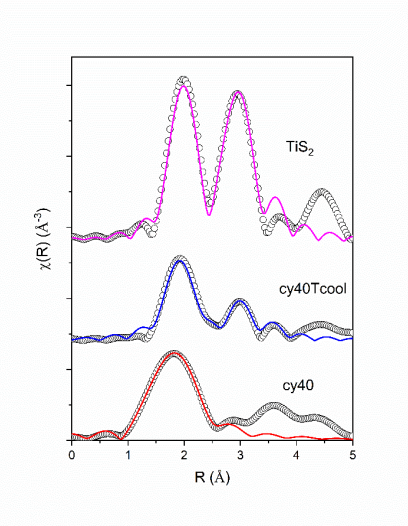

Figure S 9: The Fourier transform EXAFS spectra (scatter points) and its corresponding fits (solid line) for metal-organic film (cy40) after 40 cycles and after cooling the sample. The Fourier transform spectra of standards TiS_2 is also shown for reference purpose.

Table S 1: Bond lengths calculated from DFT optimized mono-podal structures simulated using different potentials and Van der Walls correlations.

Bond	**PBE**	**PBEsol**	**vdw-optb88**	**vdw-optPBE**	**vdw-rev-DF2**
Ti-O	1.9829	1.97461	1.93422	1.96952	1.96650
Ti-N1	1.9029	1.88257	2.34744	1.90456	1.89467
Ti-N2	1.9115	1.89315	1.97878	1.91690	1.90644
Ti-N3	1.9011	1.88377	2.14206	1.90621	1.89812
N1-C6	1.4498	1.43901	1.46378	1.45578	1.44812
N1-C5	1.4572	1.4468	1.44569	1.46505	1.45699
N2-C4	1.4533	1.44247	1.41609	1.46198	1.45359
N2-C3	1.4553	1.44536	1.44310	1.46278	1.45487
N3-C2	1.4562	1.44645	1.45943	1.46304	1.45566
N3-C1	1.4520	1.44107	1.41948	1.45903	1.45157
Si-O-Ti	138.2692	136.5223	132.6495	137.4685	137.3045

Table S 2: EXAFS fitting results (bond lengths and disorder factors) from Ti K-edge for ALD/MLD cycles. Initial growth cycle (cy1), Final growth cycle (cy40), annealed (cy40T500) and cooled (cy40Tcool).

Cycle	**Scattering path**	**Bond length (Å)**	**Ratio (%) Ti-S/Ti-N**	**σ^2 (Å^2)**
cy1	Ti-O/N	1.90± 0.02		0.00756±0.0023
cy40	Ti-O/N	1.85± 0.01	38±5	0.0085±0.0021
	Ti-S	2.47± 0.005		0.01141±0.0016
cy40T500	Ti-O/N	1.91± 0.01	60±3	0.0044±0.0013
	Ti-S	2.42± 0.005		0.01141±0.0019
cy40Tcool	Ti-O/N	1.86± 0.01	32±3	0.0049±0.0018
	Ti-S	2.33± 0.005		0.01141±0.0033

Table S 3: EXAFS fitting results (bond lengths and disorder factors and coordination number) from S K-edge for ALD/MLD cycles. Initial growth cycle (cy1), Final growth cycle (cy40), annealed (cy40T500) and cooled (cy40Tcool).

Cycle	**Scattering path**	**Bond length (Å)**	**σ^2 (Å^2)**	**N**
cy40	S-C	1.87± 0.02	0.0030±0.0018	0.99±0.13
	S-Ti	2.34± 0.02	0.0019±0.0017	0.99±0.13
	S-C	2.74± 0.03	0.0019±0.0017	2.97±0.56
cy40Tcool	S-Ti	2.37± 0.03	0.0060±0.0026	1.58±0.22
	S-S	3.06± 0.02	0.0060±0.0026	3.16±0.47
	S-S	3.36± 0.02	0.0052±0.0048	1.73±0.29
TiS_2	S-Ti	2.40± 0.02	0.0054±0.0022	2.75±0.27
	S-S	3.40± 0.03	0.0054±0.0022	4.95±0.51
	S-S	3.44± 0.03	0.0053±0.0027	2.79±0.32

REFERENCES:

[1] X-Ray Absorption: Principles, Applications, Techniques of EXAFS, SEXAFS and XANES, edited by D.C. Konigsberger and R. Prince (Wiley, New York, 1988).

[2] Kelly, S.; Hesterberg, D.; Ravel, B. Analysis of soils and minerals using X-ray absorption spectroscopy. Methods of soil analysis part 5—mineralogical methods 2008, 5, 387–463.

[3] Calvin, Scott. XAFS for Everyone. CRC press, 2013.

[4] Murray, J. The S- Ti (sulfur-titanium) system. Bulletin of Alloy Phase Diagrams 1986, 7, 156–163.

[5] Jain, A.; Ong, S. P.; Hautier, G.; Chen, W.; Richards, W. D.; Dacek, S.; Cholia, S.; Gunter, D.; Skinner, D.; Ceder, G., et al. Commentary: The Materials Project: A materials genome approach to accelerating materials innovation. APL materials 2013, 1, 011002.

[6] Reinhardt, F.; Beckhoff, B.; Eba, H.; Kanngiesser, B.; Kolbe, M.; Mizusawa, M.; Muller, M.; Pollakowski, B.; Sakurai, K.; Ulm, G. Evaluation of high-resolution X-ray absorption and emission spectroscopy for the chemical speciation of binary titanium compounds. Analytical chemistry 2009, 81, 1770–1776.

[7] Carmalt, C. J.; Dinnage, C. W.; Parkin, I. P.; White, A. J.; Williams, D. J. Thiolate derivatives of titanium (iv) and tantalum (v) as precursors to metal sulfides. Journal of the Chemical Society, Dalton Transactions 2001, 2554–2558.